Applied Thermal Engineering 137 (2018) 545–554

Contents lists available at ScienceDirect

Applied Thermal Engineering

journal homepage: www.elsevier.com/locate/apthermeng

Research Paper

Techno-economic analysis of a reheated humid air turbine

Pau Lluis Orts-Gonzalez, Pavlos K. Zachos*, Giovanni D. Brighenti

Propulsion Engineering Centre, School of Aerospace, Transport and Manufacturing, Cranfield University, Cranfield MK43 0AL, Bedfordshire, United Kingdom

HIGHLIGHTS

- Economiser and recuperator dictate the economic metrics of a reheated humid air turbine system.
- Fuel and equipment purchase cost drive the average cost of the power produced by the system.
- Humid air turbine shows 14% higher thermal efficiency than a typical combined gas-steam plant.
- Humid air turbine show roughly 62% lower total purchasing cost than a combined gas-steam plant.

ARTICLE INFO

Keywords:
Humid air turbine
Evaporative gas turbine
Economic analysis
Power generation

ABSTRACT

The purpose of this paper is to identify the economic potential of a reheated humid air turbine system for power generation applications. A parametric analysis is performed to correlate the technology level of the system with the required cost of the electricity for economic viability. The effect of fluctuations of the main cost drivers is evaluated via an uncertainty analysis. The performance of the studied reheated humid air turbine is compared against previously studied humid configurations and well established gas-steam combined cycles. The fuel cost is found to be driving the cost of electricity. The uncertainty analysis also shows the dependency of the optimum cycle design parameters upon the market prices. The analysis reveals the capability of the reheated humid air turbine to be an economically viable option for the power generation sector featuring an estimated cost of electricity 2.2% lower than simpler humid cycles, and 28% lower than established combined cycles currently in service. The outcome of the work constitutes a step forward in the understanding of the economic performance of advanced complex cycles and proves the potential of such systems for applications where high efficiency and economic performance is jointly required.

1. Introduction

Over the past decades, thermal efficiency enhancements in gas turbine systems have been a key driver in the development of advanced power plant configurations. Advanced gas turbine configurations previously studied include steam injection, triple-pressure combined cycles, and humid air turbines [1–5]. Although combined gas-steam cycles are currently an established option in terms of thermal efficiency, several studies have postulated that humid air systems could also be attractive in the small to medium-size power generation market [5–10].

Humid Air Turbines (HAT) or Evaporative Gas Turbines (EvGT) were initially introduced by Rao in the late 80's [11]. Jonsson and Yan [9] performed a techno-economic comparison between HATs and combined cycles. This study proved the capability of the HATs to achieve a similar cost of electricity with a lower specific investment cost. Subsequent cost studies performed by Traverso and Massardo [12], and Kavanagh and Parks [10] showed that HATs are capable to achieve a lower cost of electricity that Combined Cycle Gas Turbines (CCGT), demonstrating the techno-economic potential of this advance cycle for the power generation market. The ability of the HAT systems to recuperate a notable part of the waste heat back into the cycle without the need of a bottoming cycle is the main driver of the observed competence against the CCGTs.

Pedemonte et al. [13,14] experimentally analysed the off-design performance of the air saturator. Wang et al. [15] and Kim et al. [7] studied the effect of the ambient conditions on the performance of the HAT. In both works, it was proved that as the ambient temperature increases the performance of the HAT is less penalised than the 'dry' gas turbines or the CCGTs. During warm days, the humid cycle is capable to evaporate a larger amount of water compensating the negative effect of a poorer compressor performance. In addition, Takashi et al. [16] concluded that humid air turbines show a better efficiency than CCGTs during part-load performance across a similar range of operation. In terms of emissions, Yagi et al. [17] reported that HAT NO_x emissions

* Corresponding author. Tel.: +44 (0) 1234 75 46 33.
E-mail addresses: p.ortsgonzalez@cranfield.ac.uk (P.L. Orts-Gonzalez), p.zachos@cranfield.ac.uk (P.K. Zachos).

https://doi.org/10.1016/j.applthermaleng.2018.03.094
Received 26 September 2017; Received in revised form 7 February 2018; Accepted 28 March 2018
Available online 30 March 2018
1359-4311/ © 2018 The Authors. Published by Elsevier Ltd. This is an open access article under the CC BY license (http://creativecommons.org/licenses/BY/4.0/).

Nomenclature

Symbols

C_x	[J/K] Heat capacity
C^*	[-] heat capacity ratio
c_p	[J/kg K] specific heat capacity
COE	[$/kW h] cost of electricity
$\overline{COE}$	[$/kW h] average cost of electricity
H^+	[J/kg] enthalpy invariant
h	[J/kg] specific enthalpy
h_{fg}	[J/K] specific enthalpy of evaporation
M^+	[-] mass invariant
$\dot{m}$	[kg/s] mass flow
n	[years] years of life of the power plant
p	[Pa] pressure
p_{sat}	[Pa] saturation pressure
PEC	[$] purchase equipment cost
$\dot{Q}$	[W] heat rate
R_x	[J/kg K] specific gas constant
$SPEC$	[$/kW] specific purchase equipment cost
ΔT_{sp}	[K] saturator pinch point temperature difference
T	[K] temperature
t	[hours/year] hours of operation per year
T_{dew}	[K] wet bulb temperature
T_{sat}	[K] saturation temperature
$\dot{W}$	[W] plant power output

Abbreviations

AC	aftercooler
AE	annual expenses
CEPCI	chemical engineering plant cost index
DC	direct costs
EC	economiser
EvGT	evaporative gas turbine
FCI	fixed capital investment
HAT	humid air turbine
IC	intercooler
Int	interests
LNG	liquid natural gas
O&M	operation and maintenance
PFI	plant fixed investment
RC	recuperator
RHAT	reheated humid air turbine
SAT	saturator
TCI	Total Cost of Investment

Subscripts

a	dry air
$comb$	combustor
$comp$	compressor
fin	financing
g	humid air
gen	generator
HX	heat exchangers
i	operational year
in	inlet
ini	initial
max	maximum
min	minimum
out	outlet
v	vapour
w	water

Greek Symbols

η_{th}	thermal efficiency
ε	effectiveness
Ξ	[$] cost
ϕ	relative humidity
ω	water to air ratio

can be as low as roughly 10 ppm due to the high content of water within in the combustion chamber. Moreover, HAT systems are more compact power-units compared with 'dry' gas turbine packages and CCGT and present faster start-up times.

Although previous studies have focused on the performance capabilities of HAT systems, little effort has been invested to understand the full techno-economic potential of this cycle. Chiesa et al. [18] suggested that the addition of a reheater in the gas turbine would augment the thermal efficiency and specific work of the power plant. A reheated HAT system was previously studied by Brighenti et al. [19]. This work confirmed the potential of the reheated HAT configuration to achieve thermal efficiencies beyond the threshold of 60%. Nevertheless, no economic study of the reheated HAT system has been presented so far to identify the economic viability of such a system.

This paper presents a techno-economic analysis of a 40 MW class reheated humid air turbine power plant for power generation. A parametric design space exploration is performed to demonstrate the impact of the heat exchanger technology level on the economic metrics. An uncertainty analysis showing the impact of the main cost driver fluctuations on the cost of the electricity is also included. Finally, the economic performance of the investigated cycle is benchmarked against the performance achieved by high efficiency humid and combined cycle systems previously presented.

2. Methodology

2.1. Cycle configuration and modelling approach

The Reheated Humid Air Turbine (RHAT) analysed in this study, shown in Fig. 1, is based on the configuration previously presented by Brighenti et al. [19]. The cycle layout includes an aftercooler to augment the saturator performance as proposed by Thern et al. [20], an

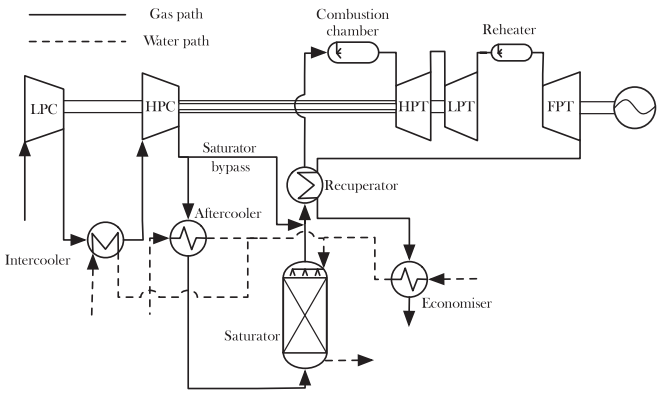

Fig. 1. Reheated humid air turbine system cycle layout.

intercooler to minimise the compression work, and an economiser to raise the temperature of the feeding water, as discussed by Nyberg and Thern [21]. A saturator bypass is included between the exit of the high pressure compressor and the inlet of the combustion chamber as suggested by Ågren and Westermark [22,23]. An open loop is used to feed water in the heat exchangers as previously discussed by Rosen [24].

The thermal performance of the system is simulated using a computational platform comprising modules that estimate the thermal behaviour of each component of the RHAT system. This platform has been previously described in detail by Brighenti et al. [19]. The performance of the gas turbine and the recuperator is calculated by Turbomatch© [25], a zero-dimensional, modular, component-based simulation framework developed at Cranfield University. The performance of the turbines and compressors are calculated using the polytropic expansion/compression relationships, the efficiency definitions, and the enthalpy balances. The performance of the combustor is estimated the enthalpy balance and the assumed efficiency of the burner. Details about the modelling approach for the main parts of the gas generator, i.e. compressors, turbines and burners, are shown by Walsh and Fletcher [26]. The performance calculation platform has been extensively validated in previous studies [27–30]. The performance of the saturator is calculated using the model based on mass and energy balance, in addition to mass and heat transfer equations, presented by Brighenti et al. [19]. This model has been also validated against experimental data provided by Lindquist et al. [31]. The key equations of the saturator performance calculation method adopted herein as well as the validation of the method is shown in Appendix A. The outlet conditions from all air-water heat exchangers and the recuperator unit are calculated using their imposed effectiveness and the energy balance equations as shown in Appendix B. The simulation platform also includes the calculation of the required turbine blade cooling flows, bled at the outlet of the high pressure compressor. The approach developed by Young and Wilcock in [32] has been employed for the estimation of the turbine cooling requirements.

The required parameters for the definition of the cycle are presented in Table 1, together with their assumed values. The bypass ratio, heat capacity ratio of the heat exchangers, and relative pressure ratio are optimised to maximise the thermal efficiency of the cycle, according to the model presented by Brighenti et al. [19]. The bypass ratio of the saturator is an optimised variable that varies across a range between 0 and 1, the relative pressure ratio from 0.25 to 0.75, and the air-water heat exchanger's heat capacity ratio from 0.3 to 0.95. The effectiveness of the heat exchangers is used as the technology level indicator of the cycle. The heat exchanger technology level scenarios analysed are shown in Table 2 and include a low, an average, and a high technology level case in terms of heat exchanger effectiveness. The optimised cycle parameters for each heat exchanger technology scenario are shown in Table 3.

Table 1
Cycle performance modelling assumptions.

Power output	40 MW
Turbine inlet temperature for both combustion chambers	1600 K
Overall pressure ratio	40
Compressor polytropic efficiency	0.90
Core turbine polytropic efficiency	0.90
Power turbine polytropic efficiency	0.92
Combustion chamber efficiency	0.99
Combustion chamber pressure loss	5%
Saturator pinch point	5 K
Saturator pressure loss	5%
Water-air heat exchangers air-side pressure loss	7.5%
Cold-side recuperator pressure loss	7.5%
Hot-side recuperator pressure loss	5%
Maximum allowed blade metal temperature	1300 K
Film cooling effectiveness	0.40
Internal flow cooling efficiency	0.70

Table 2
Heat exchanger effectiveness envelopes analysed.

Parameter	Technology level		
	Low	Average	High
Intercooler, Aftercooler, Economiser effectiveness	0.75	0.85	0.95
Recuperator effectiveness	0.8	0.85	0.90

Table 3
Optimised parameters for the studied cycle configurations.

Parameter		Technology level		
		Low	Average	High
Saturator bypass ratio	$\dot{m}_{g,AC}/\dot{m}_{g,HPC}$	0.46	0.41	0.53
Relative low pressure ratio	$\frac{\log PR_{LPC}}{\log OPR}$	0.57	0.53	0.53
Intercooler's heat capacity ratio	C_g/C_w	0.95	0.95	0.95
Aftercooler's heat capacity ratio	C_g/C_w	0.95	0.95	0.95
Economiser's heat capacity ratio	C_g/C_w	0.88	0.88	0.82

2.2. Cost analysis method

The economic analysis of the system relies on the Purchase Equipment Cost (PEC) as an economic metric to define the acquisition price. This comprises the cost of the gas generator including the power turbine ($\Xi_{bare\ GT}$), the packaging ($\Xi_{packaging}$), the electric generator (Ξ_{gen}), the saturator tower (Ξ_{SAT}), and the heat exchangers ($\sum \Xi_{HX}$), as shown in Eq. (1). The total price of the bare gas turbine includes the compressors, the turbines, the combustion chambers, and the ancillaries, as shown in Eq. (2). The acquisition cost of the turbomachinery and the electric generator are estimated using the correlations presented by Traverso et al. [33]. The cost of the compressors (Ξ_{comp}) and turbines (Ξ_{turb}) is based on the inlet mass flow, pressure ratio, inlet temperature and the assumed polytropic efficiency. The cost of the combustion (Ξ_{comb}) chamber is based on the outlet temperature, the temperature raise, and the relative pressure losses. The cost of the generator (Ξ_{gen}) is correlated with the power generated. The cost of the ancillaries ($\Xi_{ancillaries}$) is assumed to be 40% of the turbomachinery cost, and the cost of the packaging is estimated as 40% the cost of the previous two, as suggested by Kavanagh [10].

$$PEC = \Xi_{bare\ GT} + \Xi_{packaging} + \Xi_{gen} + \Xi_{SAT} + \sum \Xi_{HX} \quad (1)$$

$$\Xi_{bare\ GT} = \sum \Xi_{comp} + \sum \Xi_{turb} + \sum \Xi_{comb} + \Xi_{ancillaries} \quad (2)$$

The acquisition cost of the saturator is estimated based on the weight of the shell (8800 USD/ton) and the packing volume (3800 $/m^3), assuming that both are made in stainless steel as recommended by Lindquist in [34]. To account for the cost of the droplet eliminator, water sprays, and the rest of the subcomponents an additional $14,000 is added on top of the baseline cost [34]. The main dimensions of the saturator are calculated using the model presented by Brighenti et al. [19] (also in Appendix A of this paper) for a structured packing-bed configuration.

The intercooler, the aftercooler, and the recuperator are plate-fin counter-current cross-flow units, whereas the economiser is designed as a finned-tube counter-current cross-flow unit to avoid passage blocking as a consequence of water condensation, according to the configuration presented by Brighenti et al. [19]. The acquisition cost of the heat exchanger is estimated based on the heat transfer area using the correlations presented by the ESDU [35] for the plate-fin units, and by Casarosa [36] for the finned-tube units. The total heat transfer area of the heat exchangers is calculated using the effectiveness-Number of Transfer Units method developed by Kays and London [37]. Unit costs

Table 4
Economic assumptions for the calculation of the total cost of investment [40].

Total cost of investment	Fixed capital investment	Direct costs	Installation	20% of PEC
			Piping	10% of PEC
			Instruments and control systems	6% of PEC
			Electric equipment and materials	10% of PEC
			Land	5% of PEC
			Civil, structural, and architectural work	15% of PEC
			Service facilities	30% of PEC
		Indirect costs	Engineering and supervision	25% of PEC
			Construction	15% of DC
			Contingency	8% of all the above
	Other outlays		Startup	8% of FCI
			Working capital	15% of FCI
			Licensing, and research and development	7% of FCI

known from previous years are updated to 2015 prices using the Chemical Engineering Plant Cost Index (CEPCI) as described in [38]. The detailed heat exchanger geometry is specified using the methodology previously presented by Brighenti et al. [19].

In the absence of any detailed data about the infrastructure required, the Total Cost of Investment (TCI) is estimated based on the Purchasing Equipment Cost (PEC), the Direct Costs (DC), and the Fixed Capital Investment (FCI), as suggested by Bejan et al. [39]. The assumed values of these costs are based on the work published by Barberis et al. [40] and are represented in Table 4.

For a lifecycle economic analysis, the annual expenses during the plant economic life are required. These are estimated using the model proposed by Bejan et al. [39] which accounts for the payment of the Total Cost of Investment (TCI), the interest generated by the required loan (cost of financing), the taxes, the cost of fuel, and the Operation and Maintenance (O&M) costs to estimate the annual expenses (C_{AE_i}) as shown in Eq. (3). The TCI accounts for the plant's sub-system's costs including installation costs, the land acquistion costs, the construction of the access roads, etc. The loan's interests are derived from the credit required to pay off the TCI. In this study the loan is divided in three parts, a part paid with a common equity, other with debt, and the other with preferred stock. The fuel costs include the purchase of fuel required to operate the power plant, which is based on the power and efficiency of the plant. Finally, the O&M costs include the mantime required for normal operation of the power plant as well as the maintenance costs over the lifetime of the system including the costs for replacement parts. In this study, the O&M costs include a fixed part proportional to the PEC and a part proportional to the fuel used. Full details about the cost model can be seen in [39].

The assumed values to enable the cost study are presented in Table 5. The analysis is conducted in current dollars accounting for inflation and the assumptions made to support it rely on the economy of a developed country. A similar study using economic figures of an emerged economy might be able to identify the potential of such an advanced cycle system as part of the energy market in a developing country where high efficiency plants are also of critical importance.

Table 5
Assumptions for economic analysis.

Assumed starting year of the project	January 2015
Time until commissioning starts	1 year
Assumed plant commissioning time	2 years
Plant economic life	20 years
Plant life for tax purposes	10 years
Income tax rate	30%
Other taxes and insurances	2% of PFI
Real inflation	2.5%
Real inflation for the fuel	3.0%
Fraction funded by common equity	35%
Fraction funded by preferred stock	15%
Fraction funded by debt	50%
Interest rate of the common equity	6.5%
Interest rate of the preferred stock	6.0%
Interest rate of the debt	5.5%
Fuel price (LNG)	0.25 $/kg
O&M variable	2% of FCI
O&M fixed	0.83 $/kg of fuel
Availability	85%

The Cost of Electricity (COE) is calculated using Eq. (4). The COE_i represents the total cost of generating a kilowatt hour at year i and reflects the minimum sale price to recover the annual expenses. The COE varies during the book life of the power plant following the annual cost variation. As such, the average cost of electricity, $\overline{COE}$, for the book life is used as an economic index and is calculated as shown in Eq. (5). Average cost of electricity represents the total average cost of generating one kilowatt hour accounting for the annual expenses along the whole book life.

$$\Xi_{AE_i} = \Xi_{ini_i} + \Xi_{fin_i} + \Xi_{tax_i} + \Xi_{fuel_i} + \Xi_{O\&M_i} \tag{3}$$

$$COE_i = \frac{\Xi_{AE_i}}{t\dot{W}} \tag{4}$$

$$\overline{COE} = \frac{\sum_{i=1}^{n} C_{AE_i}}{nt\dot{W}} \tag{5}$$

3. Results and discussion

3.1. Effect of heat exchanger technology

The effect of the heat exchanger effectiveness on the thermal efficiency and the economic metrics of the power plant is presented in Fig. 2 for the three scenarios shown in Table 2. In this study the Specific Purchase Equipment Cost ($SPEC$) and the average cost of electricity ($\overline{COE}$) of the average technology scenario (heat exchanger effectiveness at 0.85 for all units, $SPEC$ = 334.06 $/kW, $\overline{COE}$ = 6.81 c$/kW h) have been used as reference to calculate relative changes. Fig. 2 shows that a

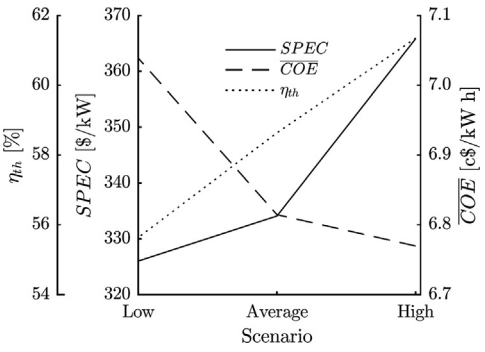

Fig. 2. Impact of the technology level of the heat exchangers on the $\overline{COE}$, $SPEC$, and η_{th}.

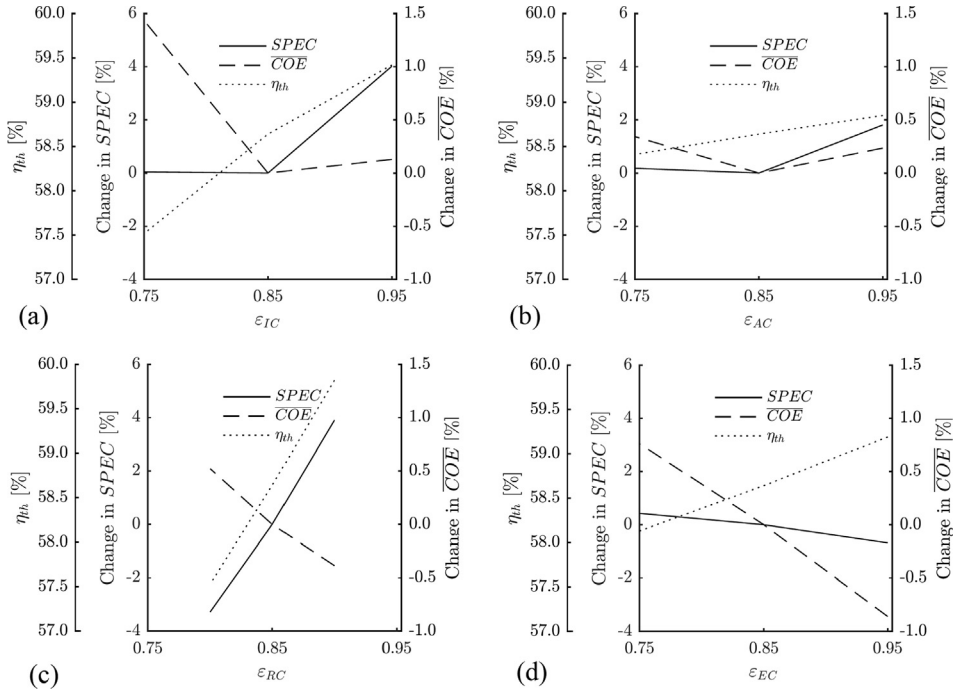

Fig. 3. (a) Effect of the intercooler, (b) effect of the aftercooler, (c) effect of the recuperator, (d) effect of the economiser effectiveness on η_{th} on *SPEC* and on $\overline{COE}$.

reduction in the heat exchanger effectiveness from the average to the low technology level is associated with a 2.3% reduction in the Specific Purchasing Equipment Cost (*SPEC*), which when combined with the 3 percentage points (pp) loss in thermal efficiency yields to a 3% increase of the $\overline{COE}$. Improving the heat exchanger technology from the average to the high level scenario (see Table 2) yields to a more aggressive change in *SPEC*, which increases by 9.5% in this case. This increase combined with the improvement in thermal efficiency yields to a 1% reduction of the $\overline{COE}$ relative to its baseline value.

The impact of the effectiveness of each heat exchanger on the thermal efficiency, *SPEC*, and $\overline{COE}$ is shown in Fig. 3. The effectiveness of each heat exchanger varies across its specified design range, in order to identify its relative contribution to the overall economic metrics of the system, while the rest of the design variables are kept constant.

Fig. 3a shows that the reduction of the intercooler effectiveness from 0.85 to 0.75 causes an increase in the average cost of electricity by 1.46%. Although this reduction doesn't affect the purchasing costs of the unit, a notable penalty on its thermal efficiency is imposed, which drops by approximately 1 pp from 58.6%. Poor air humidification and the higher required compression work promoted by the less effective intercooling reduces the specific power of the plant causing an increase in size. Therefore, the lower acquisition cost of the less effective intercooler is compensated by the higher price of the rest of the units which keeps the *SPEC* fairly constant. An intercooler effectiveness of 0.95 drives the system to more efficient but also to higher *SPEC* configurations, which effectively cancel each other out leaving the average cost of electricity almost unaffected. The aftercooler shows broadly a similar behaviour as the intercooler (see Fig. 3b). However, the changes in *SPEC* and thermal efficiency triggered by the increase in effectiveness are found to have a secondary effect on the predicted $\overline{COE}$. A 5 pp reduction in recuperator effectiveness (0.8 from 0.85, Fig. 3c) entails a 0.5% increase in the predicted $\overline{COE}$ due to the associated penalties in thermal efficiency (−1.34 pp) which are not compensated by the almost 4% reduction in *SPEC*. The driver behind the thermal efficiency deterioration is the reduced capacity of the system to exploit the waste heat. For a 5 pp increase in recuperator effectiveness (0.9 from 0.85), the thermal efficiency gain (+1.18 pp) out-competes the 4% increase in *SPEC* yielding to 0.5% reduction in the $\overline{COE}$. Finally, the economiser is found to also drive the cost of electricity across a ± 1% zone for effectiveness values of 0.75 and 0.95 respectively. This change is primarily dominated by the increase in thermal efficiency of the system produced by a more effective unit.

Table 6
Heat exchanger effectiveness for minimum average cost of electricity ($\overline{COE}$).

ε_{IC}	[–]	0.85
ε_{AC}	[–]	0.85
ε_{RC}	[–]	0.90
ε_{EC}	[–]	0.95
η_{th}	[%]	60.33
SPEC	[$/kW]	345.33
$\overline{COE}$	[c$/kW h]	6.74

In conclusion, the analysis shows that the recuperator and the economiser primarily drive the cost metrics of the power plant, while the intercooler has a big impact on cost only for low effectiveness values. The parametric analysis enables the identification of the most cost-efficient system configuration. This features an intercooler and aftercooler effectiveness of 0.85, economiser effectiveness 0.95, and recuperator effectiveness 0.90 (see Table 6). The identified values of heat exchanger effectiveness that produce the cost optimum configuration balance the capacity of the cycle to recuperate heat directly against its capacity to exploit un-recuperated waste heat to raise humidity.

3.2. Uncertainty analysis

The total annual cost of the power plant operation depends on four key parameters: (i) fuel costs, (ii) purchase equipment costs (PEC), (iii)

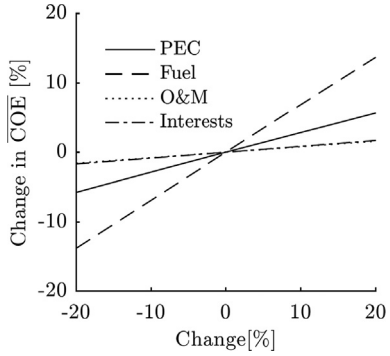

Fig. 4. $\overline{COE}$ sensitivities in cost drivers for the most cost efficient configuration.

interest rates over the loan period to pay off the initial investment, and (iv) operation and maintenance (O&M) costs. The nature of these cost elements is associated with an implicit uncertainty. Fuel prices may undergo severe fluctuations over time following global financial trends. Purchase cost estimates rely on correlations derived statistically from public domain data with an implicit standard deviation. The assumed interest rates may change significantly depending on the risk of the economic project, which is declared by the investor and heavily influenced by the current financial conditions. Finally, the O&M costs can vary across a wide range depending on the technology level of the equipment installed, the location of the power plant, operation mode, ambient conditions as well as other unforeseen circumstances which need to be accounted for as contingency. According to the above considerations, an imposed variation, across a range between −20% to +20%, is applied to each of the four parameters over the lifetime of the plant aiming to to assess the sensitivity of the average cost of electricity on these cost drivers. The selected uncertainty range is based on the expected error ranges derived from the calculation methods shown by Traverso et al. [33] and Bejan et al. [39] which justify that such a range is representative for the type of cost studies presented herein. The cycle configuration shown in Table 6 is used as reference to show the variations of the $\overline{COE}$. The reference values of interest rates, baseline fuel cost, and the O&M costs are the presented in Table 5, whereas the baseline purchase equipment cost (PEC) of $13,813,200 is derived from the *SPEC* provided in Table 6.

Fig. 4 shows the impact of the four parameters analysed on the $\overline{COE}$. The fuel cost is found to have the strongest influence in the $\overline{COE}$, showing a change of 0.75% per percentage point fuel cost variation. The PEC uncertainty causes small changes in the $\overline{COE}$, of the order of 0.25%, for each PEC percentage point variation. Variations in the O&M costs or the interest rates of the debts have minor effect, producing changes of only 0.05% per percentage point change (note that O&M and Interests lines are collapsing on top of each other in Fig. 4). Therefore, both lines appear overlapped in Fig. 4. The analysis reveals a linear correlation between any of the four cost drivers and the $\overline{COE}$. Therefore, such a study enables the impact of larger fluctuations of any of the four cost drivers by extrapolation using the data presented herein as reference.

The tile-plot shown in Fig. 5 identifies the exchange rates between all cost drivers across the design space. On each plot, the x-axis represents the percentage variation of the interest rates, and the y-axis the percentage variation of the O&M costs from the reference values shown in Table 5. Fuel cost variation from nominal values is shown in the major x-axis while uncertainty in PEC is shown in the major y-axis. The contour lines represent the percentage $\overline{COE}$ departure from the reference value (Table 6). Point A in Fig. 5 represents a pessimistic scenario whereby the variation of the four parameters is +20% with regards to their reference values. In that case, the $\overline{COE}$ is estimated to be around 23% higher with respect to the baseline case (point REF in Fig. 5). An optimistic scenario is represented by point B (bottom left corner in Fig. 5), where the variation for the four parameters is −20% in relation to their baseline values. This scenario shows a $\overline{COE}$ reduced by 22% compared to the baseline case (point Ref. in Fig. 5). In addition, as the PEC uncertainty decreases, the rate of change of the $\overline{COE}$ produced by the in interest rates and the O&M cost variations diminishes as these two parameters show strong dependence on purchasing costs. Finally, from Fig. 5 it becomes clear that increased relative fuel costs dictate a cost optimum system configuration with high technology level inter-cooler and recuperator (light grey regime ε_{IC} = 0.95, ε_{RC} = 0.90), which better exploits the waste heat within the power cycle. When the anticipated relative fuel costs drop, a low technology level system seems to also be viable (ε_{IC} = 0.85, ε_{RC} = 0.85, dark grey regime in Fig. 5), which combines low operating costs with low purchasing costs due to the relatively more compact size of these heat exchangers.

3.3. Comparison against other advanced cycles

In Table 7 the RHAT configuration shown in Table 6 is compared against the cost metrics of humid cycles previously reported by Kavanagh and Parks [10], and Traverso and Massardo [12]. A CCGT cycle [10] is also included for reference. The cost metrics of the current RHAT system are re-estimated under the assumptions of previous studies (Kavanagh et al. [10], Traverso and Massardo [12]) to enable comparison.

Table 7 shows that the RHAT system features 62% lower predicted cost of investment than an equivalent CCGT. As a result, the average cost of electricity ($\overline{COE}$) is reduced by 28%, also due to the RHAT's 14% higher thermal efficiency. Comparing against previous humid cycles, it is observed that the RHAT cycle features a 15% and roughly 8.5% lower *SPEC* than STIG and simpler HAT cycles respectively (Kavanagh and Parks [10]). The lower *SPEC* is a consequence of the higher specific power achieved by the RHAT (130% compared with the STIG and 38% compared with the HAT), as it reaches higher humidification ratios. As such, despite the additional combustion chamber and the requirement for advanced materials, the reduction in size of all the components, as a consequence of the higher specific power, enables a cost reduction that out-competes the above mentioned drawbacks. Nevertheless this reduction is not sufficiently large to achieve a lower *SPEC* than the TOP Humid Air Turbine [10], which does not require an intercooler, an aftercooler, or a humidifier. From Table 7 is also observed that the RHAT cycle out-competes the rest of the cycles in terms of thermal efficiency due to its increased capability to exploit waste heat and introduce humidity into the cycle. Finally, the enhanced thermal efficiency and the low purchasing costs of the RHAT system yield to a notably lower estimated average cost of electricity against the competitor systems with the $\overline{COE}$ reductions ranging from −28% against the CCGT plant [10] to roughly −2% against the humid air water injected system shown in [12].

4. Conclusions

In this paper, a techno-economic analysis of a reheated humid air turbine system is presented. Lifecycle cost analysis showed that the average cost of electricity is primarily driven by the effectiveness of the recuperator and economiser. These heat exchanger units represent the key components that manage the waste heat recuperation and humidity levels while they also dictate the size, hence the acquisition cost, of the power plant. Increasing the technology level of the recuperator and the

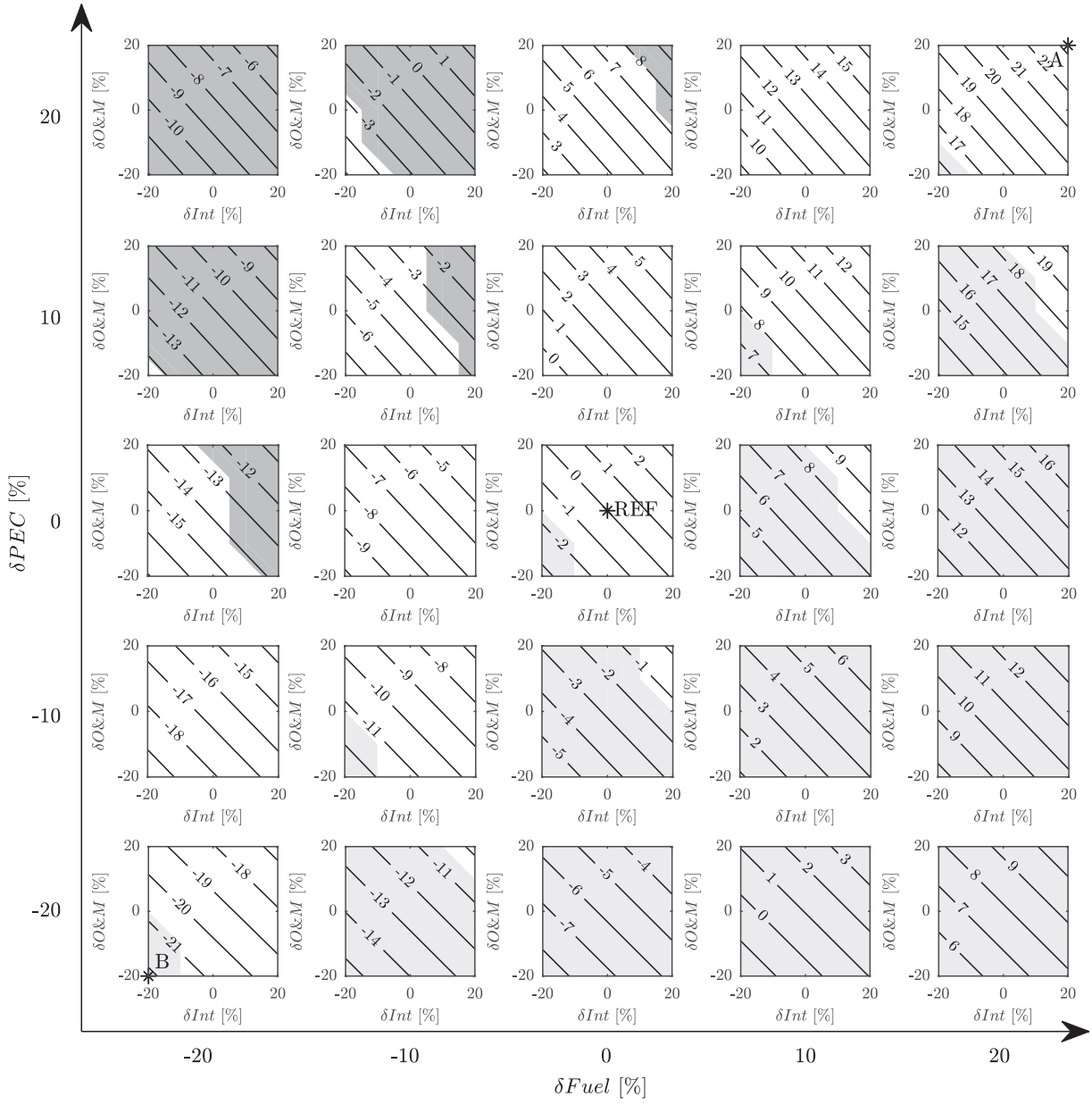

Fig. 5. Percentage mean cost of electricity variation from reference cycle. Cost optimum configuration in dark grey region $\varepsilon_{IC} = 0.85$, $\varepsilon_{AC} = 0.85$, $\varepsilon_{RC} = 0.85$, $\varepsilon_{EC} = 0.95$. Cost optimum configuration in blank region $\varepsilon_{IC} = 0.85$, $\varepsilon_{AC} = 0.85$, $\varepsilon_{RC} = 0.90$, $\varepsilon_{EC} = 0.95$. Cost optimum configuration in light grey region $\varepsilon_{IC} = 0.95$, $\varepsilon_{AC} = 0.85$, $\varepsilon_{RC} = 0.90$, $\varepsilon_{EC} = 0.95$.

Table 7
Comparison of reference reheated humid air turbine (Table 6) performance against previously reported advanced cycles.

Cycle	η_{th} [%]		*SPEC* [$/kW]		$\overline{COE}$ [c$/kW h]	
		RHAT		RHAT		RHAT
Steam injected cycle [10]	49.36	+22.2%	323	−14.9%	6.85	−26.4%
Gas-steam combined cycle [10]	53.00	+13.8%	720	−61.8%	7.00	−28.0%
Humid Air Turbine [10]	52.26	+15.4%	300	−8.3%	6.48	−22.2%
TOP Humid Air Turbine [10]	54.12	+11.5%	187	+47.0%	6.00	−16.0%
Humid Air Turbine [12]	51.74	+16.6%	n/a	n/a	4.21	−5.5%
Humid Air Water Injected Turbine [12]	50.04	+20.6%	n/a	n/a	4.07	−2.2%

economiser by 5 and 10 percentage units respectively yields to a reduction in the cost of the electricity of about 0.5% and 1% respectively.

The uncertainty study showed that possible variations in fuel costs and the uncertainty of the purchased equipment cost are the main parameters driving the fluctuations of the average cost of the electricity. The cost of electricity increases by 0.75% per percentage point of fuel price increase, and by 0.25% per percentage point rise in purchase equipment cost. Comparisons against previously reported studies

on combined and humid cycles show that the reheated humid air turbine features 61.8% lower purchasing costs than a typical CCGT. Moreover, due to its high efficiency (approximately 14% higher than a typical combined cycle), estimated average costs of electricity are approximately 30% lower than these of CCGT system.

Overall a detailed economic analysis of a reheated humid air turbine power plant intended for power generation has been performed in order to explore the potential of this configuration for power generation applications. The impact of the heat exchanger technology on the economic metrics was demonstrated, revealing their influence on the acquisition cost and in the $\overline{COE}$, which was not previously known. The outcome of the work constitutes a step forward in the understanding of the economic performance of advanced complex cycles and proves the potential of such systems for applications where high efficiency and economic performance is jointly required.

Acknowledgements

This research program is financially supported by an EPSRC Industrial CASE Award and Rolls-Royce plc. under the University Technology Centre in Aero System Design, Integration and Performance at Cranfield University. The authors kindly thank Rolls-Royce plc. for permission to publish this work. Due to confidentiality agreements with research collaborators, supporting data can only be made available upon reasonable request and with permission of the industrial collaborator. For data requests please contact the corresponding author.

Appendix A. Saturator tower performance calculation

The model for simulating the design performance of the saturator tower, previously presented by Brighenti et al. [19], relies on the inlet pressure, temperature, and mass flow of the two streams (dry air and water) and the pinch point temperature difference (ΔT_{ps}). The pinch point temperature difference is defined as the minimum temperature difference between the operating line of the water and the saturated air enthalpy line across the saturator [41]. For this modelling process, the air–vapour mixture is treated as an ideal mixture of ideal gases, while the air at the outlet of the saturator is assumed to be fully saturated [22]. From the conservation of the dry air and water mass as well as conservation of energy two invariants of the system (M^+, H^+) can be defined as:

$$\frac{\dot{m}_w}{\dot{m}_a} - \omega = M^+ \tag{6}$$

$$h_a@(T_g) + \omega[h_v@(T_g) - h_w@(T_w)] - M^+ h_w(T_w) = H^+ \tag{7}$$

Under the assumption of an ideal mixture of ideal gas, absolute humidity is defined as:

$$\omega = \frac{\phi\, p_{sat}@(T_g)}{p - \phi\, p_{sat}@(T_g)} \frac{R_a}{R_v}. \tag{8}$$

$\dot{m}$ represents the mass flows of the two streams, M^+ the mass invariant, $h_x@(T)$ the specific enthalpy evaluated at temperature T, p the pressure, ω the water to air ratio (defined as the amount of vapour in the air divided by the dry air $\dot{m}_v/\dot{m}_a$), H^+ the enthalpy invariant. $p_{sat}@(T_g)$ indicates the saturation pressure evaluated at the temperature of the gas. ϕ represents the relative humidity, R_x is the specific gas constant of each fluid, and the subscripts a, g, w, and v stand for dry air, humid air, water, and vapour respectively.

For the calculation of the saturated gas thermodynamic properties, the above-defined system of equations is solved at three sections along the saturator gas path. “Station 0” corresponds to the pinch point condition between the operating line and the saturated enthalpy line of the air. The temperature difference between the two above-mentioned lines is defined by ΔT_{ps}. Therefore, it is possible to approximate the water temperature as $T_w = \Delta T_{ps} + T_g$. “Station 1” corresponds to the bottom section of the tower, where the air inlet conditions are known. Last, “Station 2” corresponds to the top section of the saturator, where the water inlet conditions are known and the outlet air is assumed to be saturated. The equations Eq. (6)–(8) are evaluated and solved at “Station 0” and “Station 2”, which enables the calculation of the two invariants (M^+, H^+) and the conditions of the outlet gas. Once the invariants are known, the system of equations is evaluated at “Station 1”, which corresponds to the bottom section of the saturator, to calculate the conditions of the outlet water. Finally, the air outlet pressure is calculated assuming a 5% pressure loss of the inlet total pressure.

The saturator performance model was previously validated against experimental data obtained by Lindquist et al. [31] using the Lund HAT cycle demonstrator, as shown in Table 8.

Table 8
Validation of the saturator model against experimental data from Lindquist et al. [31].

Inlet/Input conditions			Outlet conditions				
Paremeter	Units	Data	Parameter	Units	Model	Experimental data	Discrepancy (%)
$m_{g,in}$	(kg/s)	2.17	$m_{g,out}$	(kg/s)	2.5685	2.55	0.7
$T_{g,in}$	(K)	346.75	$T_{g,out}$	(K)	389.97	389.15	0.2
p	(bar)	7.88	ω_{out}	(–)	0.1837	–	–
$m_{w,in}$	(kg/s)	3.48	$m_{w,out}$	(kg/s)	3.0815	3.10	0.6
$T_{w,in}$	(K)	419.35	$T_{w,out}$	(K)	347.52	352.85	1.5
ΔT_{ps}	(K)	10	–	–	–	–	–

The sizing model of the tower enables the estimation of the height and diameter of the saturator’s packing. The diameter is calculated following the correlation presented by Coulson and Richardson [42]. The pressure losses are set to 300 Pa/m and the maximum velocity is 60% of the flooding velocity to ensure stable operation and avoid water over-flood. The packing height is estimated based on a variation of the method previously proposed by Aramayo-Prudencio and Young [43]. This model enables the estimation of the saturator’s height from a given performance. The required inputs are: the characteristic dimensions of the packing-bed, the previously calculated diameter, an initial guess for the height, and the inlet conditions of both streams as inputs. The model iteratively calculates the humidifier’s performance based on the data provided and the initial guessed height, and compares the results with the humidifier thermodynamic data obtained from the cycle design. The packing height is determined

once the above-mentioned iteration reaches convergence.

Appendix B. Heat exchanger thermodynamic model

The outlet conditions from all air-water heat exchangers are calculated using the optimised heat capacity ratio (C^*), defined in Eq. (9), and the imposed effectiveness (ε), defined Eq. (10), where $\dot{Q}$ represents the heat rate. Gas mass flows are defined as part of the cycle analysis, whereas the heat exchanger water mass flows are calculated using the heat capacity ratio of the air and water streams, C^*, under the assumption that the water always presents the higher heat capacity ($C_w = C_{\max}$). As water condensation in the air stream is possible ($T_{g,out} < T_{g,dew}$), the latent heat of condensation of the water in the humid air causes variations in the heat capacity of the gas during the condensation process and generates a pinch point between the two streams within the heat exchanger (see Fig. 6).

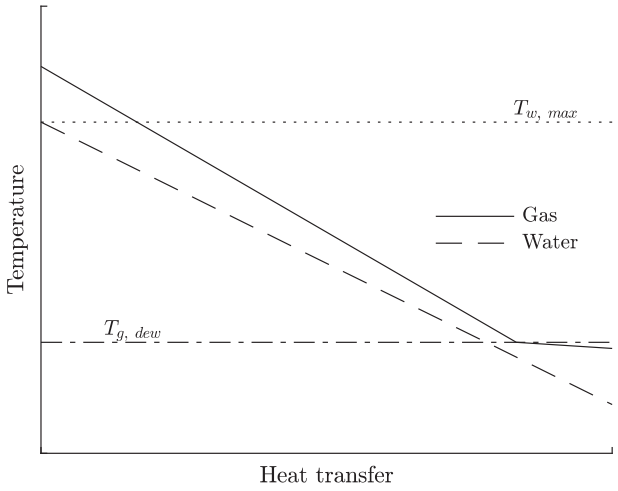

Fig. 6. Heat transfer process in air-water heat exchangers.

$$C^* = \frac{C_g}{C_w} \tag{9}$$

$$\varepsilon = \frac{\dot{Q}}{\dot{Q}_{\max}} \tag{10}$$

In order to calculate the heat exchanger outlet conditions and iterative scheme is used. The procedure begins by guessing the water mass flow. Then the maximum heat transferred ($\dot{Q}_{\max}$) is calculated as the minimum between Eq. (11) and Eq. (12). The subscripts *in* and *out* stand for inlet and outlet conditions respectively, $h@(T)$ is the specific enthalpy evaluated at temperature T and h_{fg} is the specific enthalpy of evaporation of the water.

$$\dot{Q}_{\max} = \dot{m}_{g,in} h_g@(T_{g,in}) - [\dot{m}_{g,out} h_g@(T_{w,in}) + (\dot{m}_{g,in} - \dot{m}_{g,out}) h_{fg}] \tag{11}$$

$$\dot{Q}_{\max} = \dot{m}_w h_w@(T_{g,in}) - \dot{m}_w h_w@(T_{w,in}) \tag{12}$$

Subsequently, the outlet gas and water temperatures are obtained from Eq. (13) and Eq. (14) respectively, where $\dot{Q}$ is obtained from Eq. (10).

$$\dot{Q} = \dot{m}_{g,in} h_g@(T_{g,in}) - [\dot{m}_{g,out} h_g@(T_{g,out}) + (\dot{m}_{g,in} - \dot{m}_{g,out}) h_{fg}] \tag{13}$$

$$\dot{Q} = \dot{m}_w h_w@(T_{w,out}) - \dot{m}_w h_w@(T_{w,in}) \tag{14}$$

The amount of condensed vapour is obtained from Eq. (15). $\omega_{sat}@(T_{g,out}, p_g)$ is the saturated water to air ratio evaluated at the outlet temperature of the gas and at the pressure of the gas. When $\omega_{sat} > \omega_{in}$ no condensation is taking place and the amount of water condensed is to zero.

$$\dot{m}_{g,in} - \dot{m}_{g,out} = \dot{m}_a(\omega_{in} - \omega_{out}) = \dot{m}_a[\omega_{in} - \omega_{sat}@(T_{g,out}, P_g)] \tag{15}$$

Once the outlet temperature of both flows is obtained, the heat capacity ratio of the air and water side is calculated from Eq. (16). $\Delta T_{x,dry}$ represents the temperature jump of the stream in the dry section, that is from the inlet of the gas up to the dew point. When no condensation occurs, $\Delta T_{x,dry}$ represents the temperature jump across the whole heat exchanger.

$$C_x = \frac{\dot{Q}}{\Delta T_{x,dry}} \tag{16}$$

Finally, a revised heat capacity ratio C^* is re-calculated using the values obtained from Eq. (16). In case that the calculated and the initial design values do not match, the water mass flow guess is revised and the process is repeated until convergence is reached.

The water is injected into the saturator at a liquid phase to facilitate the humidification process. The outlet temperature of the water is limited by the water saturation temperature evaluated at the saturator's pressure. A safety coefficient of 0.9 is introduced to avoid any steaming in the saturator, as shown in Eq. (17), where $T_{sat}@(0.9 p_{SAT})$ is the saturation temperature of the water evaluated at 0.9 the saturator's pressure. In case the condition was not satisfied, the water mass flow would be increased, a new heat capacity ratio is calculated which overwrites the initial value.

$$T_{w,out} \leqslant T_{w,\max} = T_{sat}@(0.9p_{SAT}) \quad (17)$$

In the recuperator, the inlet proprieties of both streams are defined. Therefore, the outlet conditions of the two streams are calculated with the definition of the effectiveness of the heat exchanger. The pressure losses of the heat exchangers are calculated analogously to the method used in the saturator since the pressure losses are imposed as a percentage on the inlet pressure.

References

[1] A.M. Bassily, Numerical cost optimization and irreversibility analysis of the triple-pressure reheat steam-air cooled GT commercial combined cycle power plants, Appl. Thermal Eng. 40 (2012) 145–160, http://dx.doi.org/10.1016/j.applthermaleng.2012.01.038.

[2] A.M. Bassily, Enhancing the efficiency and power of the triple-pressure reheat combined cycle by means of gas reheat, gas recuperation, and reduction of the irreversibility in the heat recovery steam generator, Appl. Energy 85 (12) (2008) 1141–1162, http://dx.doi.org/10.1016/j.apenergy.2008.02.017.

[3] S.K. Bakhshmand, R.K. Saray, K. Bahlouli, H. Eftekhari, A. Ebrahimi, Exergoeconomic analysis and optimization of a triple-pressure combined cycle plant using evolutionary algorithm, Energy 93 (2015) 555–567, http://dx.doi.org/10.1016/j.energy.2015.09.073.

[4] M. Jonsson, J. Yan, Humidified gas turbines—a review of proposed and implemented cycles, Energy 30 (7) (Jun. 2005) 1013–1078, http://dx.doi.org/10.1016/j.energy.2004.08.005.

[5] A. Rao, "Evaporative Gas Turbine (EvGT)/Humid Air Turbine (HAT) Cycles", Handbook of Clean Energy Systems, John Wiley & Sons Ltd, Chichester, UK, 2014.

[6] H. Araki, T. Koganezawa, C. Myouren, S. Higuchi, T. Takahashi, T. Eta, Experimental and Analytical study on the operation characteristics of the AHAT system, J. Eng. Gas Turbines Power 134 (2012), http://dx.doi.org/10.1115/1.4004732.

[7] T.S. Kim, C.H. Song, S.T. Ro, S.K. Kauh, Influence of ambient condition on thermodynamic performance of the humid air turbine cycle, Energy 25 (4) (Apr. 2000) 313–324, http://dx.doi.org/10.1016/S0360-5442(99)00074-2.

[8] M. Nakhamkin, E.C. Swensen, J.R. Scheibel, A. Cohn, CHAT Technology: an alternative approach to achieve advanced turbine systems efficiencies with present combustion turbine technology, ASME International Gas Turbine and Aeroengine Congress and Exhibition, Paper No. 98-GT-43, ASME, Stockholm, Sweden, Jun. 1998.

[9] M. Jonsson, J. Yan, Economic assessment of evaporative gas turbine cycles with optimized part flow humidification systems, in: Proceedings of ASME Turbo Expo, Paper No. GT2003-38009, ASME, Atlanta, Georgia, USA, 2003.

[10] R.M. Kavanagh, G.T. Parks, A systematic comparison and multi-objective optimization of humid power cycles—part II: economics, J. Eng. Gas Turbines Power 131 (2009), http://dx.doi.org/10.1115/1.3026562.

[11] A.D. Rao, Process for Producing Power, 1989.

[12] A. Traverso, A.F. Massardo, Thermoeconomic analysis of mixed gas-steam cycles, Appl. Thermal Eng. 22 (1) (Jan. 2002), http://dx.doi.org/10.1016/S1359-4311(01)00064-3.

[13] A.A. Pedemonte, A. Traverso, A.F. Massardo, Experimental analysis of pressurised humidification tower for humid air gas turbine cycles. part a: experimental campaign, Appl. Thermal Eng. 28 (2008) 1711–1725, http://dx.doi.org/10.1016/j.applthermaleng.2007.10.030.

[14] A.A. Pedemonte, A. Traverso, A.F. Massardo, Experimental analysis of pressurised humidification tower for humid air gas turbine cycles. Part B: correlation of experimental data, Appl. Thermal Eng. 28 (2008) 1711–1725, http://dx.doi.org/10.1016/j.applthermaleng.2007.10.030.

[15] B. Wang, S. Zhang, Y. Xiao, Steady state off-design performance of humid air turbine cycle, in: Proceedings of ASME Turbo Expo, Paper No. GT2007-27350, ASME, Montreal, Canada, 2007, pp. 139–149.

[16] T. Takahashi, Y. Nakao, E. Koda, Analysis and evaluation about advanced humid air turbine system, Challenges of Power Engineering and Environment, Springer Berlin Heidelberg, Berlin, Heidelberg, 2007, pp. 341–344.

[17] M. Yagi, H. Araki, H. Tagawa, T. Koganezawa, C. Myoren, T. Takeda, Progress of the 40 MW-class advanced humid air turbine tests, J. Eng. Gas Turbines Power 135 (11) (Sep. 2013), http://dx.doi.org/10.1115/1.4025037.

[18] P. Chiesa, G. Lozza, E. Macchi, S. Consonni, An assessment of the thermodynamic performance of mixed gas-steam cycles part B- water-injected and hat cycles, J. Eng. Gas Turbines Power 117 (3) (1995) 499–508, http://dx.doi.org/10.1115/1.2814122.

[19] G. Brighenti, P.L. Orts-Gonzalez, L. Sanchez, P.K. Zachos, Design point performance and optimization of humid air turbine power plants, Appl. Sci. 7 (4) (Apr. 2017), http://dx.doi.org/10.3390/app7040413.

[20] M. Thern, T. Lindquist, T. Torisson, Theoretical and experimental evaluation of a plate heat exchanger aftercooler in an evaporative gas turbine cycle, in: Proceedings of ASME Turbo Expo, Paper No. GT2003-38099, ASME, Atlanta, Georgia, USA, 2003, pp. 103–111.

[21] B. Nyberg, M. Thern, Thermodynamic studies of a HAT cycle and its components, Appl. Energy 89 (1) (2012) 315–321, http://dx.doi.org/10.1016/j.apenergy.2011.07.036.

[22] N.D. Ågren, M.O.J. Westermark, Design study of part-flow evaporative gas turbine cycles: performance and equipment sizing. Part II: industrial core, J. Eng. Gas Turbines Power 125 (2003) 216–227, http://dx.doi.org/10.1115/1.1476925.

[23] N.D. Ågren, M.O.J. Westermark, design study of part-flow evaporative gas turbine cycles: performance and equipment sizing. Part I: aeroderivative core, J. Eng. Gas Turbines Power 125 (2003) 201–215, http://dx.doi.org/10.1115/1.1476924.

[24] M. Rosen, Evaporative Cycles – in Theory and in Practise, PhD Thesis Lund Institute of Technology, Lund, Sweden, 2000.

[25] W.L. Macmillan, Development of a Module Type Computer Program for the Calculation of Gas Turbine Off Design Performance, PhD Thesis Cranfield University, Cranfield, UK, 1974.

[26] P.P. Walsh, P. Fletcher, Gas Turbine Performance, second ed., Blackwell Science Ltd, Oxford, UK, 2004.

[27] V. Pachidis, P. Pilidis, L. Marinai, I. Templalexis, Towards a full two dimensional gas turbine performance simulator, Aeronaut. J. 111 (1121) (Jul. 2007) 433–442, http://dx.doi.org/10.1017/S0001924000004693.

[28] Y.G. Li, L. Marinai, V. Pachidis, E.Lo Gatto, P. Pilidis, Multiple-point adaptive performance simulation tuned to aeroengine test-bed data, J. Propul. Power 25 (3) (2009) 635–641, http://dx.doi.org/10.2514/1.38823.

[29] P. Giannakakis, P. Laskaridis, T. Nikolaidis, A.I. Kalfas, Toward a scalable propeller performance map, J. Propul. Power 31 (4) (Jul. 2015) 1073–1082, http://dx.doi.org/10.2514/1.B35498.

[30] A. Pellegrini, T. Nikolaidis, V. Pachidis, S. Köhler, On the performance simulation of inter-stage turbine teheat, Appl. Thermal Eng. 113 (2017) 544–553, http://dx.doi.org/10.1016/j.applthermaleng.2016.10.034.

[31] T. Lindquist, M. Thern, T. Torisson, Experimental and theoretical results of a humidification tower in an evaporative gas turbine cycle pilot plant, in: Proceedings of ASME Turbo Expo, Paper No. GT2002-30127, ASME, Amsterdam, Netherlands, 2002, pp. 475–484.

[32] J.B. Young, R.C. Wilcock, Modeling the Air-cooled gas turbine: part 2 – coolant flows and losses, J. Turbomach. 124 (2002) 214–221, http://dx.doi.org/10.1115/1.1415038.

[33] A. Traverso, A.F. Massardo, W. Cazzola, G. Lagorio, WIDGET-TEMP: a novel web-based approach for thermoeconomic analysis and optimization of conventional and innovative cycles, in; Proceedings of ASME Turbo Expo, Paper No. GT2004-54115, ASME, Viena, Austria, 2004, pp. 623–631.

[34] T. Lindquist, Evaluation, Experience and Potential of Gas Turbine Based Cycles with Humidification, PhD Thesis Lund Institute of Technology, Lund, Sweden, 2002.

[35] ESDU, Selection and costing of heat exchangers, ESDU Data Items, No. Data Item No. 92013, 1994.

[36] C. Casarosa, F. Donatini, A. Franco, Thermoeconomic optimization of heat recovery steam generators operating parameters for combined plants, Energy 29 (3) (2004) 389–414, http://dx.doi.org/10.1016/S0360-5442(02)00078-6.

[37] W.M. Kays, A.L. London, Compact Heat Exchangers, third ed., Krieger Pub. Co, New York, USA, 1984.

[38] The Annual Cost Index of Chemical Engineering Plant, Chemical Engineering, 2015.

[39] A. Bejan, G. Tsatsaronis, M.J. Moran, Thermal Design and Optimization, John Wiley & Sons Inc, New York, USA, 1996.

[40] S. Barberis, A. Traverso, Thermoeconomic analysis of CSP air-steam mixed cycles, in: Proceedings of ASME Turbo Expo, Paper No. GT2015-42189, ASME, Montreal, Canada, Jun. 2015.

[41] A. Aramayo-Prudencio, J.B. Young, The analysis and design of saturators for power generation cycles: part 1 – thermodynamics, in: Proceedings of ASME Turbo Expo, Paper No. GT2003-38945, ASME, Atlanta, Georgia, USA, 2003, pp. 411–421.

[42] J.M. Coulson, J.F. Richardson, J.H. Harker, J.R. Backhurst, Chemical Engineering: Particle Technology and Separation Process, 5th ed., Butterworth-Heinemann, Oxford, UK, 2002.

[43] A. Aramayo-Prudencio, J.B. Young, The analysis and design of saturators for power generation cycles : part 2 – heat and mass transfer, in: Proceedings of ASME Turbo Expo, Paper No. GT2003-38946, ASME, Atlanta, Georgia, USA, 2003, pp. 423–432.

Cranfield University

CERES https://dspace.lib.cranfield.ac.uk

School of Aerospace, Transport and Manufacturing (SATM) Staff publications (SATM)

2018-03-30

Techno-economic analysis of a reheated humid air turbine

Orts-Gonzalez, Pau Lluis

Elsevier

Orts-Gonzalez PL, Zachos PK, Brighenti GD. (2018) Techno-economic analysis of a reheated humid air turbine. Applied Thermal Engineering, Volume 137, June 2018, pp. 545-554 https://doi.org/10.1016/j.applthermaleng.2018.03.094

Downloaded from Cranfield Library Services E-Repository